Chapter 5
DL-Polylactide (DL-PLA) Based Polyaniline Composite for Hydrogen Gas Sensors

Muktikanta Panigrahi [1, *], Basudam Adhikari [1]

[1] Materials Science Centre, Indian Institute of Technology, Kharagpur, West Bengal, India

*Corresponding author: muktikanta2@gmail.com

Abstract

Different inorganic acids like HCl, HNO_3, H_2SO_4 and H_3PO_4-doped based DL-PLA/PANI-ES composites were synthesized by *in-situ* chemical oxidation polymerization technique using liquid aniline as precursors. The doped composite have observed fibril-like morphology with different average sized diameter (178 nm for HCl doped composite, 162 nm (H_2SO_4 doped composite), 153 nm (H_3PO_4 doped composite) and 163 nm (HNO_3 doped composite), respectively. Analysis of presence of functional groups and other chemical groups of as prepared composites was done by FTIR experiment in ATR mode. The optical (direct) band gap was estimated from UV-Visible absorption spectra. The estimated band gap values are to be 160 eV, 1.37 eV, 1.46 eV, and 1.69 eV for HCl, HNO_3, H_2SO_4 and H_3PO_4-doped DL-PLA/PANI-ES composite, respectively. The electrical conduction mechanism of HCl-, H_2SO_4- and H_3PO_4-doped DL-PLA/PANI-ES composites were taken to study the conduction mechanism in detail in the low temperature regime (77-300 K) with and without applied of the magnetic field. Different models such as variable range hopping (VRH) and Arrhenius model were taken to explain the conduction mechanism of as prepared composites. In the Mott type VRH model, the density of states at the Fermi level, which is constant in the temperature range of 77-300 K were estimated. In the absence of magnetic field, DC conductivity of HCl-, H_2SO_4- and HNO_3-, H_3PO_4- doped DL-PLA/PANI-ES composite was measured. Also, magnetoresistance (MR) was measured at room temperature for as prepared doped DL-PLA/PANI-ES composites and showed negative MR. In addition, we were discussed the response of hydrogen (H_2) gas with polyaniline-based sensor materials.

***Keywords*:** Conducting polymer, Nanofibers, DC conductivity, VRH model, Activation energy, Magnetoresistance, Hydrogen gas response

https://doi.org/10.34256/ioriip2125

1.0 Introduction

Conductivity is a main characteristic of polymeric materials for their potential applications in different fields such as light emitting diodes, supercapacitors, sensors, [1-3]. The preparation constraints can be changed in a precise mode to get desired conductivity of the polymeric materials. Two methods such as doping and structural modification are generally used to increase the conductivity of polymeric materials. Hence, appropriate doping agent and polymeric materials prerequisite to select for improving the conductivity. In the connection, polyaniline (PANI) is one of the polymeric materials. It is commonly known as intrinsically conducting polymer (ICP). Generally, ICP is not established under ambient circumstance. Different methods are adopted to improve the stability of PANI. One of the ways is to be used to make composite form using thermoplastic polymer as base materials, which act as a stabilizer [4]. A variety of PANI composites have been prepared using different types of thermoplastic polymers such as poly (methyl methacrylate), polyvinyl chloride, polystyrene and polyurethane [5-8] as base materials. The detail electrical behaviours were studied with and without magnetic field [9-12].

To realize the conducting behaviour of different doped conducting polymer, various models are anticipated. Predominantly, variable range hopping (VRH) model is employed to understand the transport phenomena. In the connection, Li and co-workers proposed a VRH model and explained the conduction mechanism of HCl- and DBSA- doped polyaniline [13]. Kapil and co-workers [14] studied conduction mechanism of p-toluene sulphonic acid (PTSA) doped polyaniline by VRH model, Arrhenius model, and Kivelson model in the temperature range of 30−300 K. The conduction mechanism of polyaniline organic film and embedded metal particles in an insulating material were also described by VRH and charge-energy-limited-tunnelling (CELT) models. Similarly, the conductivity is measured with the variation of magnetic field at constant temperature, which is called magnetoresistance (MR). It helps to realize the depth of transport phenomena.

A few conducting polymers have shown positive MR such as PANI [15-18], polypyrrole [19-21], PEDOT films [22], and PANI composites at low temperature (0<10 K). The positive MR of conducting polymer is ascribed to the shrinkage of localised wave functions of electron in the presence of magnetic field [23] or electron-electron interactions [24,25]. Moreover, there are also a few polymers which show negative MR. Lee et al. [26] reported the negative MR from highly conducting polyacetylene at low temperature (1.5 K), which was attributed to the weak localization effects.

Our goal was to prepare an environmentally stable PANI-ES composite that would show better electrical properties and, therefore, can be potential for gas sensor and other electronic applications. We selected DL-PLA polymer in the composite preparation because of its high mechanical properties compared to other biodegradable polymer and strong interaction with ionic electroactive polymer such as PANI. Inorganic acids (HCl or H_2SO_4 or H_3PO_4) were doped into DL-PLA/PANI-ES to improve the electrical properties of the as prepared composites by *in situ*

polymerization technique. The low and room temperature conductivity of HCl, H_2SO_4 and H_3PO_4 doped DL-PLA/PANI-ES composite is investigated by DC conductivity measurement and possible conduction mechanism is proposed. Furthermore, MR of H_2SO_4 and H_3PO_4 doped DL-PLA/PANI-ES composite have been studied.

2.0 Experimental Details

2.1. Preparation Of DL-PLA Films and DL-PLA/PANI-ES Composites

During the synthesized of doped DL-PLA/PANI-ES COMPOSITES**,** small sized DL-PLA films were first prepared by solution casting method by taking DL-PLA beats and chloroform ($CHCl_3$) as polymer and polar solvent, respectively at room temperature. 2 g of DL-PLA polymer was added to 20 mL of $CHCl_3$ in a beaker (100 mL) and stirred continuously for 3 h. The transparent viscous soluble product was formed and poured into a 10 cm diameter petridish. It was left 10 h for solvent evaporation. After solvent evaporation in the petridish, DL-PLA film formed. The films removed from petridish and cut into small pieces having 1.5 cm × 1.5 cm size. It was used for synthesizing composite and raw materials characterizations.

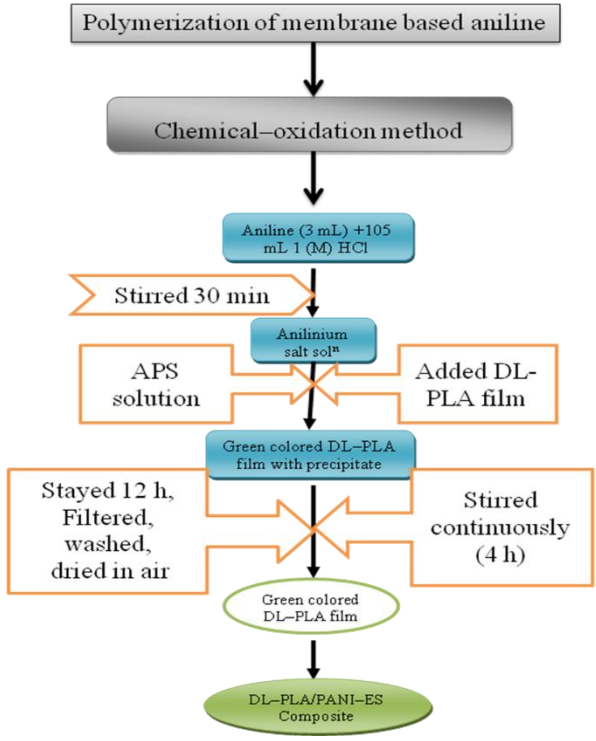

Scheme 1. The flow chart of preparation of HCl doped DL-PLA/PANI-ES composite [28]

During the doped DL-PLA/PANI-ES composites synthesized, *in situ* technique via chemical-oxidation polymerization technique was employed. The polymerization reaction was carried out at room temperature using aniline and DL-PLA film (1 cm^2), which act as monomers and base material, respectively. During the polymerization process, 3 mL of liquid aniline was taken and was added to 105 mL of aqueous 1 M HCl solution. It was stirred for 0.5 h until slightly yellowish solution was formed and the solution was called **Solution 1**. After that, DL-PLA films (1.5 cm × 1.5 cm) were put in solution 1. It was stirred for 12 h. During the preparation of s**olution 2,** 7.47 g of ammonium perdisulphate (APS) was added to 60 mL of 1 M HCl solution. The **solution 2** was added drop wise to the mixture which contained DL-PLA and solution 1 with continuous stirring for 1 h. The polymerization reaction was carried out. The color of the reaction solution and DL-PLA film was changed from white to light green and finally to dark green as polymerization continue to progress. The polymerization reaction was continued to stir constantly for 10 h to complete the polymerization reaction. HCl doped DL-PLA/PANI-ES composite was finally prepared and washed with deionised water several times followed by drying in the ambient conditions [27, **28**].

Similar process was employed to synthesize other composites (HNO_3, H_2SO_4 and H_3PO_4 doped DL-PLA/PANI-ES composites). Schematic diagram of the flow chart of HCl doped DL-PLA/PANI-ES composites is exposed (**Scheme 1)**. The prepared composites was used for different characterizations.

2.2. Characterization Techniques.

Fourier transformation infrared (FTIR) spectra were recorded in ATR mode on a Thermo Nicolt Nexus 870 spectrophotometer.

Ultra-violet visible (UV-Vis) spectra were recorded by using a Micropack UV-VIS-NIR, DH 2000.

Surface morphology was analysed by scanning electron microscopy (SEM) using Carl Zeiss Supra 40 scanning electron microscope. Gold coating was performed before doing SEM analysis.

I-V characteristics and DC conductivity was measured using linear four-probe technique at room temperature using Keithley 2400 programmable current source. According to four probe method, the resistivity (ρ) was calculated using the expression [29]

$$\rho = 2\pi S\left(\frac{V}{I}\right) \quad \text{.....(1)}$$

Here, S is the probe distance (cm), I is applied current (mA) and V is measured voltage (mV). Conductivity (σ) was calculated using the relation [29]

$$\sigma = \frac{1}{\rho} \quad \text{.....} \quad (2)$$

Temperature variation resistivity with magnetic field was measured using a linear four-probe method for better understanding of transport mechanism of the prepared composite. During the measurement, helium compressor (HC) (model HC-4E1)-sumitomo cryostat (model Gains research CO, INC) equipped with 0.8 T superconducting magnet (Lake shore electromagnet) was employed temperature controller (Lake shore 331). Keithley 220 programmable current source was used as a current source.

2.3. Results and Discussion

Fig. 1 (a), (b and c) and (d), (e), (f) indicate the SEM images of DL-PLA film, HCl, H_2SO_4 (low and higher magnification), H_3PO_4, and HNO_3 doped DL-PLA/PANI-ES composites, respectively.

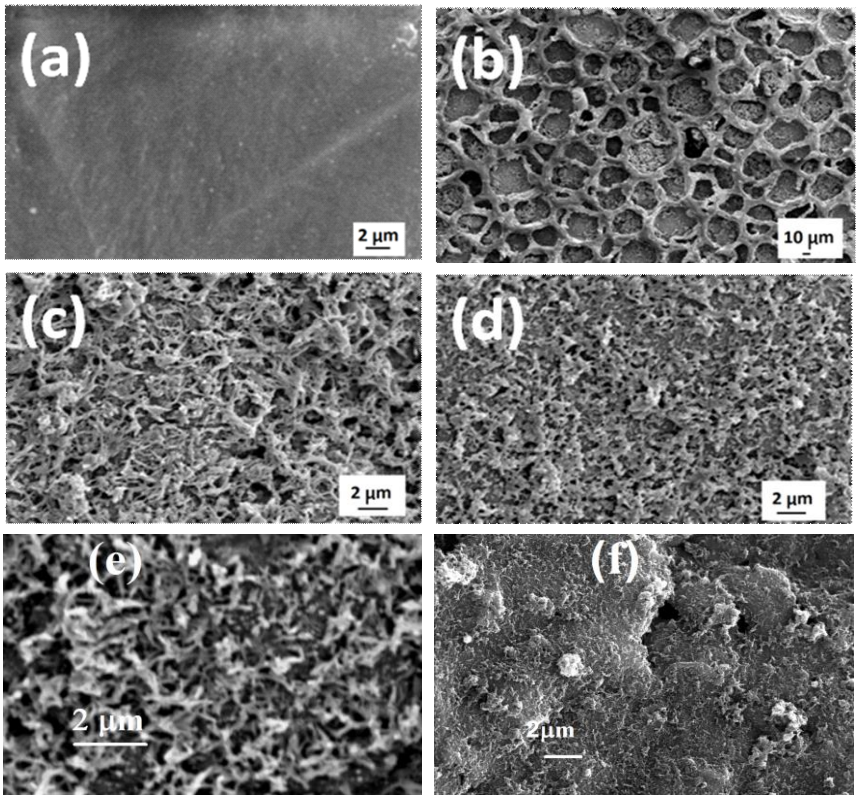

Figure 1. SEM images of (a) DL-PLA film, H_2SO_4 ((b) low and higher (c) magnification) H_3PO_4 (d), HNO_3 (e) and HCl (f) doped DL-PLA/PANI-ES composite [28]

The pure DL-PLA film appears quiet smooth (**Fig. 1a**) whereas doped DL-PLA/PANI-ES composites have fibrous morphology [**Fig. 1 (b-f)]. Fig. 1c and 1d** show the SEM images of H_2SO_4 doped DL-PLA/PANI-ES composite at two different type magnifications with a network type surface morphology (**Fig. 1c**) on the DL-PLA film. This network-type morphology is formed (**Fig. 1c**) after a DL-PLA film is put into the solution 1 (*i.e.*, before polymerization). The change in the surface morphology is believed to be due to the reaction of hydrogenium ion (from dopant) and anillium salt with ester group present in DL-PLA chain. After the polymerization (slow addition of solution 2 into the solution 1) the network type morphology remains with the formation of additional fibrous morphology all over the surface of DL-PLA film at lower magnification. The magnified image of [**Fig. 1(c)**] shows the fibrous morphology of H_2SO_4 doped DL-PLA/PANI-ES composite. The average diameter of as grown fibers was measured to be 153 nm. Similar type fibrous morphology is also obtained for H_3PO_4, HCl and HNO_3 doped DL-PLA/PANI-ES [**Fig. 1(d), 1(e) and 1(f)**] film with average fiber diameter of 163 nm, 178 nm and 162 nm, respectively. The different sized diameter is formed and it may be due to the presence of various sized counter ions in the as prepared composites. The formation of fiber morphology is favorable for the sensor application due to the inherent increase in the surface area of composite film.

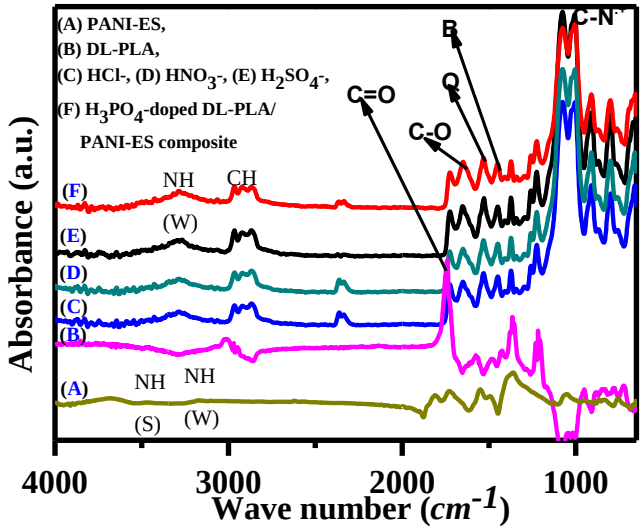

Figure 2. ATR-FTIR spectra of PANI-ES (A), DL-PLA (B), HCl (C), HNO_3 (D), H_2SO_4 (E), H_3PO_4 (F) doped DL-PLA/PANI-ES composites [28]

Fig. 2 indicates the ATR-FTIR spectra of DL-PLA, PANI-ES and HCl, H_2SO_4, H_3PO_4, HNO_3 doped DL-PLA/PANI-ES composites. All the characteristic bands and their corresponding assignments to prepare above materials are presented in **Table 1**. The absorption bands of DL-PLA at 2995, 1759, 1616 and 1216 cm^{-1} have been attributed to C-H stretching, C=O stretching, C-O stretching of ester and C-O-C

stretching vibration, respectively, whereas the bands at 1453, 1361 and 1363 cm^{-1} represent the stretching vibration of C-H deformation of DL-PLA polymer [27]. This indicates that the characteristic absorption features of DL-PLA polymer are retained in the prepared DL-PLA film. The main FTIR bands of PANI-ES are found at 1554, 1475 and 1108 cm^{-1} corresponding to quinoid, benzenoid and C=N stretching, respectively [29]. From our observation, the presence of quinoid and benzenoid ring vibrations are exhibited at 1475 and 1554 cm^{-1} respectively, indicating the presence of oxidation state of PANI-ES. The characteristic band obtained in the ATR-FTIR spectrum of DL-PLA/PANI-ES composite film indicates the formation of conducting DL-PLA/PANI-ES composite films. From **Table 1**, it is observed that N-H bands of HCl doped DL-PLA/PANI-ES, H_2SO_4 doped DL-PLA/PANI-ES, H_3PO_4 doped DL-PLA/PANI-ES appeared at 3289, 3291 and 3280 cm^{-1} respectively. The different N-H stretching peak positions represent the strong dependency on acid strength. The C=N, C=O, C-O and C-O-C stretching bands do not change significantly. The entire bands indicate that both PANI-ES and DL-PLA are retained in the composites.

Table 1. FTIR peak positions and their assignments of DL-PLA, PANI-ES, HCl, HNO_3, H_2SO_4, and H_3PO_4 doped DL-PLA/PANI-ES composites [28]

Peak assignments	**Peak positions (cm^{-1})**					
	DL-PLA	**PANI-ES**	**HCl doped DL-PLA PANI-ES**	**HNO_3 doped DL-PLA PANI-ES**	**H_2SO_4 doped DL-PLA PANI-ES**	**H_3PO_4 doped DL-PLA PANI-ES**
N−H (stretch.)	---	3217	3289	3291	3291	3280
Quinoid (stretch.)	---	1554	1533	1537	1530	1531
Benzoid (stretch.)	---	1475	1453	1450	1451	1454
C=N (stretch.)	---	1108	1067	1085	1077	1067
C−H (stretch.)	2995	2926	2965	2968	2965	2968
C=O	1759	---	1728	1720	1725	1724
C-O	1616	---	1652	1650	1656	1653
CH (def.)	1363	---	1375	1363	1374	1374
CH (bending)	1268	---	1262	1267	1259	1260
C-O-C	1216	---	1226	1223	1229	1226

It is found from literature that PANI-ES show π-π* of benzene ring, polaron to π*, benzenoid to quinoid ring and polaron transition respectively [30]. It is noticed from **Fig. 3 (A)** that there is no transition in DL-PLA film [31]. Various transitions are observed in HCl, HNO_3, H_2SO_4 and H_3PO_4 doped DL−PLA/PANI-ES composites, which is shown in **Fig. 3**. Its peak positions with their assignments are mentioned in **Table 2**. From the **Fig. 3** and **Table 2**, we found two types of bands such as π to localised polaron band and π-π* band of benzenoid ring for HCl, HNO_3, H_2SO_4 and H_3PO_4 doped DL-PLA/PANI-ES composite. Both π-π* band of benzenoid ring and polaron band are suggested to the presence of anilinic unit and oxidation unit in emeraldine salt form of composite films [30, 32]. The different peak positions and also peak areas may be happened due to the presence of a variety of nano regime PANI-ES chains on DL-PLA polymer film. This indicates the conjugation lengths which affect the band gap energy. Hence, electrons are delocalised in the excitation band [32].

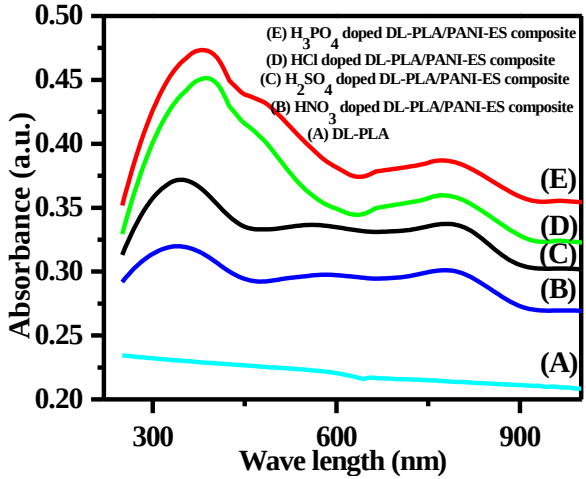

Figure 3. UV-V is spectra of neat DL-PLA (A), HNO_3 (B), H_2SO_4 (C), HCl (D), and H_3PO_4 (E) doped DL-PLA/PANI-ES composites [28]

The photon absorption in UV-Vis region of semiconducting materials is observed by Tauc expression [33]

$$\alpha h\nu = A\left(h\nu - E_g\right)^n \ldots\ldots\ldots\ldots\ldots\ldots\ldots\ldots\ldots\ldots(1)$$

Where α = Optical absorption co-efficient, hυ = photon energy, E_g = Energy gap calculated from graph, A = absorption constant, n = Represents types of transition occurs. n = 2 indicated allowed indirect transitions and n =1/2 indicated allowed direct transitions. We have plotted $(\alpha h\upsilon)^2$ *vs.* hν for direct band energy analysis of prepared samples and are shown in **Fig. 4**. It extrapolated the linear portion of it to α = 0 value to obtain direct band gap energy. The band gap energy value is found to be 1.60 *eV* for HCl doped DL-PLA/PANI-ES composite, 1.69 *eV* for HNO_3 doped DL-PLA/PANI-ES composite, 1.46 *eV* for H_3PO_4 doped DL-PLA/PANI-ES composite

and 1.37 *eV* for H_2SO_4 doped DL-PLA/PANI-ES composite, respectively. The difference in band energy occurred due to the effect of acid strength during the formation of PANI-ES on DL-PLA polymer film. It is observed from **Table 2**, the H_2SO_4 doped DL-PLA/PANI-ES composite showed highest band gap value than other three prepared composites. It may be happened due to the higher strength of H_2SO_4. It forms higher conjugation of PANI-ES chains and affect the band gap energy [30-33].

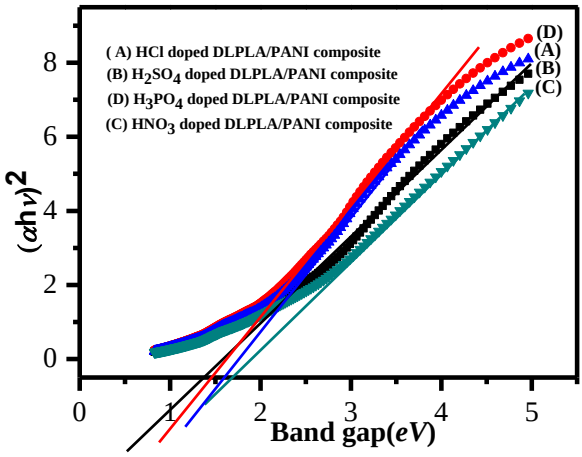

Figure 4. Optical (direct) band gap of HCl (A), H_2SO_4 (B), HNO_3 (C), H_3PO_4 (D) doped DL-PLA/PANI-ES composites [28]

Table 2. UV-Visible peak positions and their assignments and direct band gap of DL-PLA, HCl, HNO_3, H_2SO_4, H_3PO_4 doped DL-PLA/PANI-ES composites [28]

Materials	**Polaron band**	**π-π***	**Band gap (*eV*)**
DL-PLA	---	---	---
HCl doped DL-PLA/PANI-ES composite	780	383	1.60
H_2SO_4 doped DL-PLA/PANI-ES composite	797	344	1.37
H_3PO_4doped DL-PLA/ PANI-ES composite	787	381	1.46
HNO_3 doped DL-PLA/ PANI-ES composite	791	344	1.69

The DC conductivity of HCl, HNO_3, H_2SO_4, and H_3PO_4 doped DL−PLA/PANI-ES composites along with DL-PLA polymer film was measured at room temperature using linear four-probe technique. The used expression is $\sigma = 1/\rho$, ρ is resistivity. The resistivity was measured from the relation $\rho = 2\pi S\ (V/I)$, where

S is the probe spacing (0.15 cm) I is the supplied current (in nA) and V is the corresponding voltage (in mV). **Fig. 5** shows the *I-V* characteristics of HCl, HNO_3, H_2SO_4 and H_3PO_4 doped DL−PLA/PANI-ES composites at room temperature. The measured *I-V* characteristics show the linear behaviour. The linear fit straight line passes through origin indicating the ohmic behavior. The conductivity measured from *I-V* data for the HCl, HNO_3, H_2SO_4 and H_3PO_4 doped DL−PLA/PANI-ES composites is presented in **Table 3**. The conductivity of H_2SO_4 doped DL−PLA/PANI-ES composite (0.15×10^{-2} S/cm) is found to be higher than that of HCl, HNO_3, and H_3PO_4 doped DL−PLA/PANI-ES composite (0.285×10^{-4}, 0.774×10^{-3} and 0.309×10^{-3} S/cm). This could be due to that stronger H_2SO_4 dopant, which exerts more force towards better ordering of PANI polymer chains leading to higher conjugation. The conjugation is a favorable factor for the intramolecular mobility of charged species along the chains and to some extent on the intermolecular hopping because of proper arrangement of polymeric chains [34]. Additionally, H_2SO_4 doped composite produces more semiquinone conducting group and PANI-ES as compared to HCl, HNO_3 and H_3PO_4 doped composite because of highly reactive nature of H_2SO_4 dopant [35, 36].

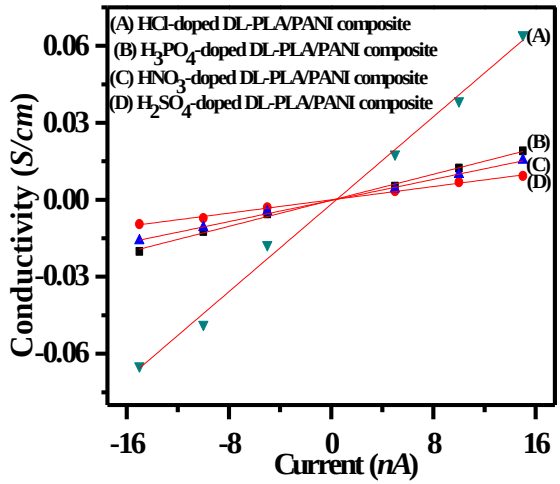

Figurer 5. DC conductivity of HCl (A), H_2SO_4 (B), HNO_3 (C) and H_3PO_4 (D) doped DL-PLA/PANI-ES composites measured at room temperature [28]

The temperature dependent DC conductivity is shown in **Fig. 6**. It shows the conductivity of HCl, H_2SO_4 and H_3PO_4 doped DL−PLA/PANI-ES composites as a function of temperature. It is evident from **Fig. 6** that the composites showed increase in conductivity with increase in the temperature from 77 to 300 K, which is similar to an inorganic semiconductor. Hence, it can be called as organic semiconductor [37].

Various models including variable range hopping (VRH) were used as to understand the probable mechanism of current transport in the organic semiconductor [38-41].

Table 3. DC conductivity of HCl, H_2SO_4, HNO_3 and H_3PO_4 doped DL-PLA/PANI-ES composites at room temperature [28]

Materials Name	**DC Conductivity (S/cm)**
DL-PLA	6.05×10^{-15}
HCl doped DL-PLA/ PANI-ES composite	0.285×10^{-4}
H_2SO_4 doped DL-PLA/ PANI-ES composite	0.162×10^{-2}
H_3PO_4 doped DL-PLA/ PANI-ES composite	0.1097×10^{-3}
HNO_3 doped DL-PLA/ PANI-ES composite	0.774×10^{-3}

According to VRH, the temperature (T) dependence of DC conductivity follows the Mott's expression [38-41].

$$\sigma = \sigma_0 \exp\left(-\frac{T_0}{T}\right)^r \text{.....(2)}$$

Where T_0 is the Mott characteristic temperature and σ_0 the limiting value of conductivity at infinite temperature and the exponent 'r' is related to the dimensionality of the transport process *via* the expression r = 1/(1+d) here, d = 1, 2 and 3 for one-, two-, and three-dimensional (1D, 2D and 3D) conduction process, respectively. Out of three processes, three dimensional processes are more fitted.

Plot (a) and (b) in **Fig. 7** show the 3D-VRH plots and Arrhenius plots on measured conductivity in logarithmic scale for HCl, H_2SO_4 and H_3PO_4 doped DL−PLA/PANI-ES composites in the temperature range of 77−300 K, respectively. The conductivity data were carefully fitted linearly to both the 1D- and 3D-VRH as well as Arrhenius plots for conduction processes. The obtained regression values are presented in **Table 4**. It is clear from **Table 4** that Mott's 3D VRH model of as prepared composite fits better into the experimental data (Regression values) than that of 1D model and Arrhenius model. This suggests that charge carrier can hop both in between the chains, *i.e.*, interchain hopping and along the chain, *i.e.*, intrachain hopping as PANI has the chain structure [38-41].

In the 3D−VRH model, the temperature dependence of DC conductivity can be written as

$$\sigma = \sigma_0 \exp\left(-\frac{T_0}{T}\right)^{\frac{1}{4}} \text{.....(3)}$$

Fig. 7 (a) shows that the linear dependence of $\ln \sigma$ *vs* $T^{-\frac{1}{4}}$ is better than that of $\ln \sigma$ *vs* $T^{-\frac{1}{2}}$. The estimated linear factor, *i.e.*, regression values (R-values) for 3D−VRH model (0.9976) was better than that of 1D−VRH model (0.974), supporting the reported literature [42-45]. T_0 and σ_0 values were also calculated from the VRH plot of H_2SO_4 doped DL−PLA/PANI-ES composite and presented in **Table 5**. Unlike the H_2SO_4 doped, the regression value for H_3PO_4 doped DL−PLA/PANI-ES composite was measured to be almost same, *i.e.*, 0.9937 and 0.993 from the 3D and 1D fitted VRH model, respectively. This indicates that 3D VRH model can be applied to describe the conduction mechanism in the H_3PO_4 doped DL−PLA/PANI-ES composite. In the H_2SO_4 doped DL−PLA/PANI-ES composite, sulphuric acid (H_2SO_4) is strong dopant which exerts stronger force leading to alignment of chains and increase in the compactness [34]. Therefore, charge carriers could hop easily from one chain to another chain obeying the 3D−VRH conduction mechanism model.

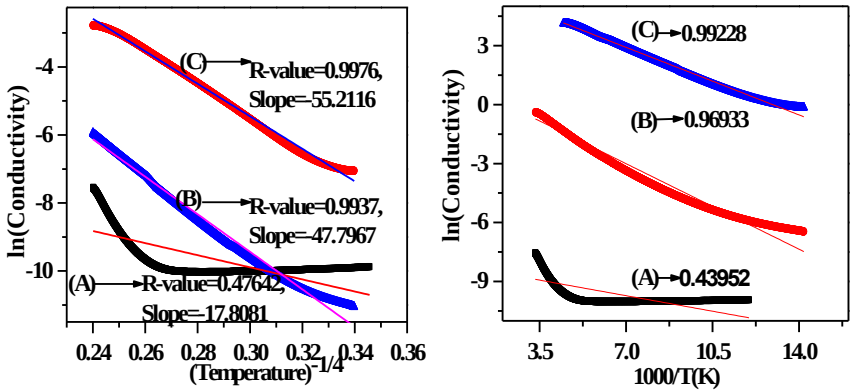

Figure 7. 3D VRH plot (left side) and Arrhenius plot (right side) of HCl (A), H_2SO_4 (B) and H_3PO_4 (C) doped DL−PLA/PANI-ES composites [28]

Other than the regression values, other parameters like density of states, hopping distance, hopping energy is supported to understand the conduction mechanism. Estimation of localisation length (L_{loc}) is an important parameter for the calculation of density of states, hopping distance, and hopping energy. Resistivity of HCl, H_2SO_4 and H_3PO_4 doped DL−PLA/PANI-ES composite was measured as a function of temperature in presence of magnetic field (0.4 T). We analyzed the resistivity data at 0.4 T (**Fig. 8**) along with the 3D−VRH model described by Mott's law [13] and given below and calculated localization length (L_{loc}) and density of states. Using these important parameters, we calculated hopping distance ($R_{hop,\ Mott}$) and hopping energy ($\Delta_{hop,\ Mott}$). The above estimated parameters help to understand the transport phenomenon.

$$\rho(T) = \rho_0 e^{\left(\frac{T_{Mott}}{T}\right)^{\frac{1}{4}}} \quad \text{.....(4)}$$

$$T_{Mott} = \frac{16}{\left[K_B N(E)_F L^3_{loc}\right]} \quad \text{.....(5)}$$

Where K_B is the Boltzmann constant, $N(E_F)$ is the density of states at the Fermi level, and L_{loc} is the localization length. The plot of $\ln \rho$ *vs* $T^{-\frac{1}{4}}$ exhibits a straight line for HCl, H_2SO_4 and H_3PO_4 doped DL−PLA/PANI-ES composites (**Fig. 8**). T_{Mott} can be evaluated from the slope of the straight line and is listed in **Table 5**. The localization length L_{loc} can also be calculated from magnetoresistivity data as shown in **Fig. 8**. From the VRH model, the resistivity at different temperatures at a particular magnetic field can be written as [46]

$$\ln\left[\frac{\rho(H)}{\rho_0}\right] = t\left(L_{loc}/L_H\right)^4\left(\frac{T_{Mott}}{T}\right)^{\frac{3}{4}} \quad \text{.....(6)}$$

Where $t = \frac{5}{2016}$, and $L_H = \left[\frac{hc}{2\pi eH}\right]^{\frac{1}{2}}$ is magnetic length, c = velocity of light (3×10^{10} cm/s), h = Planks constant (6.62×10^{-27} erg.sec), e = electronic charge (1.6×10^{-19} C) and H = 0.4 T is the applied magnetic field. From the slope of curves in **Fig. 8**, we determined the L_{loc} values and listed in **Table 5**.

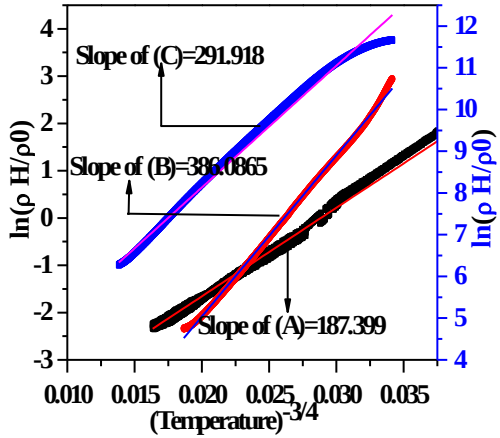

Figure 8. Plots of [lnρ(H)/ρ(0)] *vs* $T^{-4/3}$ for HCl (A), H_2SO_4 (B), H_3PO_4 (C) doped DL-PLA/PANI-ES composite at 0.4 T (77-300 K) [28]

Using the $T_{0,Mott}$ and L_{loc} of HCl, H_2SO_4 and H_3PO_4 doped DL−PLA/PANI-ES composite in equation (5), the density of states $(N(E_F))$ can be calculated.

The $T_{0,Mott}$, L_{loc}, and $(N(E_F))$ values were used to calculate the mean hopping distance R_{hop} and the energy difference between sites (Δ_{hop}) by using the following expression [13, 46] and presented in **Table 5**.

$$R_{hop,Mott} = \left(\frac{3}{8}\right)\left(\frac{T_{Mott}}{T}\right)^{\frac{1}{4}} L_{loc} \quad \text{.....(7)}$$

$$\Delta_{hop,Mott} = \left(\frac{1}{4}\right)(k_B T)\left(\frac{T_{Mott}}{T}\right)^{\frac{1}{4}} \quad \text{.....(8)}$$

By putting required parameters in the above expressions, the $R_{hop,Mott}$ and $\Delta_{hop,Mott}$ values were calculated at M-I transition temperature (125 K), which is presented in **Table 5**. In addition, the obtained hopping parameters were found to satisfy the 3D−VRH criteria.

Table 5. VRH conduction parameters obtained by analyzing the low temperature resistivity (with and without magnetic field) data of HCl, H_2SO_4, H_3PO_4 doped DL-PLA/PANI-ES composites [28]

Conducting parameters	L_H (Magnetic Length in °A)	HCl doped DL-PLA / PANI-ES composite	H_2SO_4 doped DL-PLA / PANI-ES composite	H_3PO_4doped DL-PLA/ PANI-ES composite
Slope at 0 T (3D-VRH)	49.39	-17.8081	-55.21167	-47.7966
Slope at 0.4T		187.399	386.08	291.918
T_{Mott} (*K*)		1.005×10^5	9.29×10^6	5.21×10^6
L_{loc} (°A)		95.11	48.48	50.28
N (E_F) (no. states/*eV*/*cm*^{3})		2.14×10^{18}	1.755×10^{17}	2.08×10^{17}
$R_{Hop, Mott}$ (°A) at 125 K		189.74	300.18	269.47
$\Delta_{Hop, Mott}$ (*meV* at 125 K)		19.34	44.48	38.49
Temp. at M-I (*K*)		125	125	125

Newly, the negative MR of hopping systems has been explored and various possible way of hopping path was interpreted by quantum interference effect of spins in presence of magnetic field [47-50]. This effect is ascribed to the statistics of self-crossed trajectories in conductors, *i.e.*, phase coherence of the electron's wave function between different conduction paths is destroyed in presence of magnetic field [26]. In the present work, the low temperature conductivity has indicated the hoping conduction mechanism but not the weak localization system. The concept of weak localisation effect is valid for diffusive motion of current carriers, and can be extended to hopping conduction [47, 48]. In the weak field region, the negative MR can be expressed as [47, 48].

$$MR = \left[\frac{R(H) - R(0)}{R(0)}\right] \alpha \; -H^{x}T^{-y} \quad \ldots\ldots\ldots\ldots\ldots\ldots\ldots\ldots (9)$$

Where the exponent x = 1[47] or x = 2 [48] $y = \frac{3}{4}$ for 3D – and $y = \frac{3}{2}$ for 1D−VRH. The interesting observation was found by Sivan et al. [47] and predicted quadratic field dependence over most of the weak-field range. Also, Nguyen et al. [48] reported the negative MR, which is linear in the field. Using equation (9), MR values of H_2SO_4 and H_3PO_4 doped DL−PLA/PANI-ES composites was calculated at room temperature. **Fig. 9** shows the plot of negative MR as a function of magnetic field (H). In the case of H_2SO_4 doped DL−PLA/PANI-ES composites, MR were found to linearly decrease with increase in the magnetic field whereas in case of H_3PO_4 doped DL−PLA/PANI-ES composites, the MR value was found to slightly increase above 0.4T. The above negative MR results are in qualitative agreement with the predicated features [47, 48].

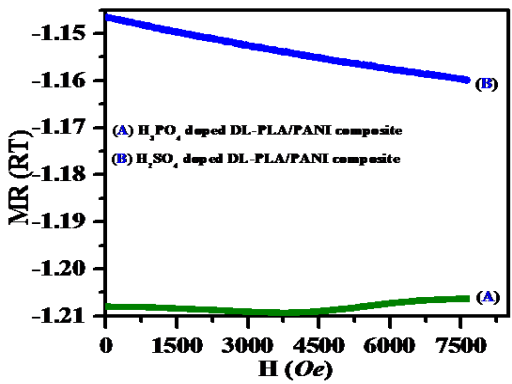

Figure 9. Magnetoresistance (MR) of H_3PO_4 (A) and H_2SO_4 (B) doped DL-PLA/PANI-ES composites at room temperature [28]

2.4. Response Of Hydrogen (H_2) Gas (i.e., H_2 Gas Sensor)

Hydrogen (H_2) is one of the flammable gases. Also, H_2 gases are found to be highly explosive. It is becoming the fuel of the next generation of automobiles. Therefore, the detection of low concentration i.e., ppm level of H_2 is highly essential in houses, vehicles, or industrial places is potentially important. The prominence of environmental gas monitoring system is well understood and much research has focused on the development of suitable sensor material [49]. In addition, Hydrogen is the cleanest, sustainable and renewable energy carrier for future fuel. Hydrogen gas is flammability when H_2 gas comes in presence 4% air or more [50]. Hence monitoring systems are essential to sense hydrogen gas at room temperature. Most of the monitoring systems available on the market are metal oxide semiconductor based sensors, which is operated at high temperature. The obtained sensor sensitivity and selectivity is significant [51-53]. The researcher is focused much more on room temperature operated sensor system. Some reports are available on conducting polymer based sensors.

Table 6. Brief summary of H_2 detection

Study	**Materials**	**Perporfa mce**	**Optimum temperat ure (^{0}C)**	**Limitation**
Conn et al. [65]	polyaniline-platinum oxide	Response time 25 s	Room Temperatu re	High H_2 Concentrat ion
Sadek et al. [66]	Polyaniline (PANI) nanofiber	Response time xxx	Room Temperatu re	High H_2 concentrati on
Conn et al. [49]	Polyaniline	Response time 20 s	Room Temperatu re	High H_2 concentrati on
Sadek et al. [67]	Polyaniline Nanofiber	Response time 28 s	Room Temperatu re	High H_2 concentrati on
Al-Mashat et al. [68]	Graphene/Polyaniline Nanocomposite	Sensitivity 1 %	Room Temperatu re	High H_2 concentrati on
Arsat et al. [68]	Ordered polyaniline nanofibers		Room Temperatu re	High H_2 concentrati on
Sandaruw an et al. [70]	Polyaniline/palladiumnano hybrids	Frequency change	Room Temperatu re	High H_2 concentrati on

The benefits of the conducting polymers have sensitive layer of gases, intrinsic conductivity, fast response, low cost, light weight, ease of synthesis, stability in air and particularly, their sensitivity at the room temperature [54-56]. Few reports

are mentioned that conducting polymers may have ability to store hydrogen [57, 58]. Polyaniline is one of the members of conducting polymer family. Since, it has chemically stable and easy to synthesize. Polyaniline can exist as two different emeraldine forms. One is called polyaniline emeraldine base, which is insulating ($\sigma \sim 10^{-5}$ S/cm) and other one is polyaniline emeraldine salt, which is metallic in nature ($\sigma < 1000$ S/cm). The metallic nature is obtained by doping process [59-64]. Both classes are completely different with their own chemical and physical properties. The unique nature of this attractive class of polyaniline highlights its potential importance in a new type of H_2 reaction. Due to versatile nature of polyamine, it is used as an active layer for H_2 gas sensors. Brief summary of H_2 gas detection is presented in Table 6.

2.4 Conclusions

HCl, H_2SO_4, HNO_3, and H_3PO_4 doped DL-PLA/PANI-ES composites were synthesized successfully by *chemical-oxidation* polymerization process. The composites showed different diameter sized fibrous morphology. Presences of preferred groups of the composites are observed from ATR-FTIR spectra. Emeraldine salt form of the composites is found from UV-Visible spectra. Room temperature I-V characteristics of the doped composites have shown ohmic behaviour. Among the composites, H_2SO_4 doped DL-PLA/PANI-ES composite (0.15×10^{-2} S/cm) was found to be higher room temperature DC conductivity than that of HCl (0.285×10^{-4} S/cm) and H_3PO_4 doped (0.309×10^{-3} S/cm) DL-PLA/PANI-ES composite. Also, the DC conductivity of as prepared composites was observed to increase as a function of temperature. In Mott's 3D-VRH model, the temperature variation DC conductivity data's are more fitted and explained the conduction mechanism of the doped composites. The temperature variation (77-300 K) resistivity measurement of HCl, H_2SO_4 and H_3PO_4 doped DL-PLA/PANI-ES composites with magnetic field (0.4 T) were performed. The L_{loc} was estimated and found to be 95.11, 48.48 and 50.28 °A for HCl, H_2SO_4 and H_3PO_4 doped DL-PLA/PANI-ES composites, respectively. Using the resistivity at 0.4 T data's and 3D-VRH model data's of as prepared composites, different conduction mechanism parameters such as $N(E_F), T_{Mott}, L_{loc}, R_{hop}, and$ Δ_{hop} were estimated. In particulars, hydrogen gas responses and mechanism of polyaniline based materials were studied.

3.0 Acknowledgments

The author conveys their sincere thanks to the CRF, IIT Kharagpur for their providing testing facilities and Materials Science Centre to do the research work. I would like to thank Prof. Debabrat Pradhan for their invaluable guidance, advices, constant inspiration and technical support to the work.

4.0 References

[1] Burroughes, J.H., Bradley, D.D.C., Brownn, A.R., Marks, R.N., Mackay, K., Friend, R. H., Burns, P. L., and Homes, A. B. (1990), Light-emitting Diodes Based on Conjugated Polymers, Nature, Vol. 347, pp. 539-541.

[2] Frackowiak, E., Khomenko, V., Jurewicz, K., Lota, K., and Beguin F. (2006), Supercapacitors Based on Conducting Polymers/Nanotubes Composites, Journal of Power Sources, Vol. 153, pp. 413-418.

[3] Conn, C., Sestak, S., Baker, A.T., and Unsworth. J. (1998), A Polyaniline-Based Selective Hydrogen Sensor, Electroanalysis, Vol. 10, pp. 1137-1141.

[4] Abdelkader, R., Amine, H., and Mohammed, B. (2012), Thermally Stable Forms of Pure Polyaniline Catalyzed by Acid-exchanged Montmorillonite Clay called Maghnite–H^+ as an Effective Catalyst, International Journal of polymer science, Vol. 2012, pp. 1-7.

[5] Yang, S., and Ruckenstein, E. (1993), Processable Conductive Composites of Polyaniline/Poly (alkyl methacrylate) Prepared via an Emulsion Method, Synthetic Metals, Vol. 59, pp. 1-12.

[6] Singh, V., Mohan, S., Singh, G., Pandey, P.C., and Prakash, R. (2008), Synthesis and Characterization of Polyaniline-carboxylated PVC Composites: Application in Development of Ammonia Sensor, Sensors and Actuators, B, Vol. 132, pp. 99-106.

[7] Okubo, M., Fujii, S., and Minami, H. (2001), Production of Electrically Conductive, Core–shell Polystyrene/Polyaniline Composite Particles by Chemically Oxidative Seeded Dispersion Polymerization, Colloid and Polymer Science, Vol. 279, pp. 139-145.

[8] Spirkova, M., Stejskal, J., and Quadrat, O. (1999), Electrically Anisotropic Polyaniline-Polyurethane Composites, Synthetic Metals, Vol. 102, pp. 1264-1265.

[9] Aleshin , A., Kiebooms, R., Menon, R., and Heeger, A.J. (1997), Electronic Transport in Doped Poly (3,4-ethylenedioxythiophene) Near the Metal-Insulator Transition, Synthetic Metals, Vol. 90, pp. 61-68.

[10] Shklovskii, B.I. and Efros, A.L. (1984), Electronic Properties of Doped Semiconductors, *(*Berlin: Springer).

[11] Long, Y.Z., Yin, Z.H., and Chen, Z.J. (2008), Low-Temperature Magnetoresistance Studies on Composite Films of Conducting Polymer and Multiwalled Carbon Nanotubes, Journal of Physical Chemistry C, Vol. 112, pp. 11507-11512.

[12] Zuppiroli, L., Bussac, M.N., Paschen, S., Chauvet, O., and Forro. L. (1994), Hopping in Disordered Conducting Polymers, Physical Review B, Vol. 50, pp. 5196-5203.

[13] Li, J., Fang, K., Qiu, H., Li, S., and Mao, W. (2004), Micromorphology and Electrical Property of the HCl-doped and DBSA-doped Polyaniline, Synthetic Metals, Vol. 142, pp. 107-111.

[14] Kapil, A., Taunk, M., and Chand, S. (2010), Preparation and Charge Transport Studies of Chemically Synthesized Polyaniline, Journal of Materials Science: Materials in Electronics, Vol. 21, pp. 399-404.

[15] Reghu, M., Yoon, C.O., Moses, D., Smith, P., Heeger A. J., and Cao, Y. (1995), Magnetoresistance in Polyaniline Networks Near the Percolation Threshold, Synthetic Metals, Vol. 69, pp. 271-272.

[16] Clark, J.C., Ihas, G.G., Rafanello, A.J., Meisel, M.W., Reghu M., Yoon, C.O., Cao, Y., and Heeger, A.J. (1995), Resistivity and Magnetoresistance of Metallic Polyaniline and Polypyrrole at Millikelvin Temperatures, Synthetic Metals, Vol. 69, pp. 215-216.

[17] Long, Y., Chen, Z., Zhang, X., Zhang, J., and Liu, Z. (2004), Synthesis and Electrical Properties of Carbon Nanotube Polyaniline Composites, Applied Physics Letters, Vol. 85, pp. 1796-1798.

[18] Sangeeth, C.S.S., Jiménez, P., Benito, A.M., Maser, W.K., and Menon, R. 2010, Charge Transport Properties of Water Dispersible Multiwall Carbon Nanotube-Polyaniline Composites, Journal of Applied Physics, Vol. 107, pp. 103719-103723.

[19] Abou-Elazab, T.F., Migahed, M.D., Park, H., Park, Y.W., MacNeillis, P., and Rabenau, T. (1996), Magnetoresistance of Polypyrrole and Polyacetylene, Synthetic Metals, Vol. 76, pp. 281-284.

[20] Mativetsky, J.M., and Datars, W.R. (2002), Morphology and Electrical Properties of Template-synthesized Polypyrrole Nanocylinder, Physica B, Vol. 324, pp. 191-204.

[21] Park, J.G., Lee, S.H., Kim, B. and Park, Y.W. (2002), Electrical Resistivity of Polypyrrole Nanotube Measured by Conductive Scanning Probe Microscope: The Role of Contact Force, Applied Physics Letters, Vol. 81, pp. 4625-4627.

[22] Aleshin, A., Kiebooms, R., Menon, R., and Heeger, A.J. (1997), Electronic Transport in Doped Poly (3,4-ethylenedioxythiophene) near the Metal-Insulator Transition, Synthetic Metals, Vol. 90, pp. 61-68.

[23] Nath, C., and Kumar, A. (2013), Effect of Temperature and Magnetic Field on the Electrical Transport of Polyaniline Nanofibers, Journal of Applied Physics, Vol. 113, pp. 093707-0937010.

[24] Long, Y., Chen, Z., Shen, J., Zhang, Z., Zhang, L., Huang, K., Wan, M., Jin, A., Gu, C., and Duvail, J.L. (2006), Magnetoresistance Studies of Polymer Nanotube/Wire Pellets and Single Polymer Nanotubes/Wires,

Nanotechnology Vol. 17, pp. 5903-5911.

[25] Long, Y., Huang, K., Yuan, J., Han, D., Niu, L., Chen, Z., Gu, C., Jin, A., and Duvail, J.L. (2006), Electrical Conductivity of a Single Au/Polyaniline Microfiber, Applied Physics Letters, Vol. 88, pp. 162113-162116.

[26] Lee, P.A., and Ramakrishnan, T.V. (1985), Disordered Electronic Systems, Reviews of Modern Physics, Vol. 57, pp. 287-337.

[27] Panigrahi, M., Singh, N.K., Gautam, R.K., Banik, R.M., and Maiti, P. (2010), Improved Biodegradation and Thermal Properties of Poly(lactic acid)/Layered Silicate Nanocomposites**,** Composite Interfaces, Vol. 17, pp. 143-158.

[28] Panigrahi, M., Pradhan, D., Majumdar, S.B., and Adhikari, B. 2017, Investigation of DC Conductivity, Conduction Mechanism and CH4 Gas Sensor of Chemically Synthesized Polyaniline Nanofiber Deposited on DL-PLA Substrate, Edited by Sanjay K. Nayak, Smita Mohanty, Lakshmi Unnikrishnan, pp. 101 -126, Trends and Applications in Advanced Polymeric Materials https:// doi.org/10.1002/9781119364795.ch6.

[29] Mathai, C.J., Saravanan, S., Anantharaman, M.R., Venkitachalam, S., and Jayalekshmi, S. (2002), Effect of Iodine Doping on the Band Gap of Plasma Polymerized Aniline Thin Films, Journal of Physics D*:*Applied Physics, Vol. 35, pp. 2206-2210.

[30] Nascimento, do G.M., Constantino, V.R.L., and Temperini, M.L.A. , 2002, Spectroscopic Characterization of New Type of Conducting Polymer-Clay Nanocomposite, Macromolecule, Vol. 35, pp. 7535-7537.

[31] Bocchini, S., and Frache, A. 2013, Comparative Study of Filler Influence on Polylactide Photooxidation**,** e-XPRESS Polymer Letters Vol.7, pp. 431-442.

[32] Shi, J., Wu, Q., Li, R., Zhu, Y., Qin, Y., and Qiao, C. (2013), The pH-Controlled Morphology Transition of Polyaniline from Nanofibers to Nanospheres, Nanotechnology, Vol. 24, 175602-17569.

[33] Ansari, A.A., Khan, M.A.M., Khan, M.N., Alrokayan, S., Alhoshan, A.M., and Alsalhi, M.S. 2011, Optical and Electrical Properties of Electrochemically Deposited Polyaniline/CeO_2 Hybrid Nanocomposite Film, Journal of Semiconductors, Vol. 32, pp. 043001-043006.

[34] Lux, F. (1994), Properties of Electronically Conductive Polyaniline: A Comparison Between Well-known Literature Data and Some Recent Experimental Findings, Polymer, Vol. 35, pp. 2915–2936.

[35] Langer, J. J., Krzyminiewski, R., Krucznski, Z., Gibinski, T., Czajkowski, I., and Framski, G. (2001), EPR and Electrical Conductivity in Microporous Polyaniline, Synthetic Metals, Vol. 122, pp. 359-362.

[36] Li, J., Fang, K., Qiu, H., Li, S., and Mao, W.J. (2004), Micromorphology and

Electrical Property of the HCl-doped and DBSA-doped Polyaniline, Synthetic Metals, Vol. 142, pp. 107-111.

[37] Chakraborty, G., Gupta, K., Meikap, A.K., and Jana, P.C. (2010), Direct Current Electrical Transport and Magneto Transport Properties of Polyaniline Nanocomposites, Journal of Physical Science, Vol. 14, pp. 207-218.

[38] Long, Y., Chen, Z., Shen, J., Zhang, Z., Zhang, L., Huang, K., Wan, M., Jin, A., Gu, C., and Duvail, J.L. (2006), Magnetoresistance Studies of Polymer Nanotube/Wire Pellets and Single Polymer Nanotubes/Wires, Nanotechnology, Vol. 17 pp. 5903-5911.

[39] Wang, Z.H., Javadi, H.H.S., Ray, A., Macdiarmid, A.G., and Epstein, A.J. (1990), Electron Localization in Polyaniline Derivatives, Physical Review B (Rapid communication), Vol. 42, pp. 5411-5414.

[40] Li, W., and Wan, M. (1998), Porous Polyaniline Films with High Conductivity, Synthetic Metals, Vol. 92, pp. 121-126.

[41] Chakraborty, G., Gupta, K., Rana, D., and Meikap, A.K. (2012), Effect of Multiwalled Carbon Nanotubes on Electrical Conductivity and Magnetoconductivity of Polyaniline, Advance Nature Science: Nanoscience Nanotechnology, Vol. 3, pp. 035015-035023.

[42] Ghosh, M., Barman, A., Meikap, A.K., De, S.K., Chatterjee, S., and Chattopadhyay, S. K. (2000), Electrical Resistivity and Magnetoresistivity of Protonic Acid (H_2SO_4 and HCl)-Doped Polyaniline at Low Temperature, Journal of Applied Polymer Science, Vol. 75, pp. 1480-1486.

[43] Faran, O., and Ovadyaho, Z. (1998), Magnetoconductance in the Variable-Range-Hopping Regime due to a Quantum-Interference Mechanism, Physical Review B, Vol. 38, pp. 5457-5465.

[44] Baumgartner, G., Carrard, M., Zuppiroli, L., Bacsa, W., Heer, W. A., and Forro, L. (1997), Hall Effect and Magnetoresistance of Carbon Nanotube Films, Physical Review B, Vol. 55, pp. 6704-6707.

[45] Yosida, Y. and Oguro, I. (1999), Variable Range Hopping Conduction in Bulk Samples Composed of Single-Walled Carbon Nanotubes, Journal of Applied Physics, Vol. 86, pp. 999-1003.

[46] Fuhrer, M. S., Holmes, W., Richards, P.L., Delany, P., Louie, S.G., Zettl, A. (1999), Nonlinear Transport and Localization in Single-Walled Carbon Nanotubes, Synthetic Metals, Vol. 103, pp. 2529-2532.

[47] Nguyen, V.L., Spivak, B.Z., and Shklovskii, B.I. (1985), Aharonov-Bohm Oscillation with and Superconductivity Flux-Quanta in Hopping Conduction, Soviet Physics-Journal of Experimental and Theoretical Physics, Vol. 62, pp. 1021-xxx.

[48] Sivan, U., Entin-Wohlman, O., Imry, Y. (1988), Orbital Magnetoconductance in the Variable-Range-Hopping Regime. Physical Review Letter, Vol. 60, pp. 1566-1569.

[49] Conn,C., Sestak, S., Baker, A.T., and Unsworth, J. 1998, A Polyaniline-Based Selective Hydrogen Sensor; Electroanalysis, Vol. 10, pp. 1137-1141.

[50] Samarasekara, P. 2009, Hydrogen and Methane Gas Sensors Synthesis of Multi-Walled Carbon Nanotubes, Chinese Journal of Physics, Vol. 47, pp.361-369.

[51] Sadek, A.Z., Wlodarski, W., Kalantar-Zadeh, K., Baker, C., and Kaner, R.B. 2007, Doped and Dedoped Polyaniline Nanofiber based Conductometric Hydrogen Gas Sensors; Sensors and Actuators A Vol. 139, pp.53-57.

[52] Sadek, A.Z., Wlodarski, W., Shin, K., Kaner, R.B., and Kalantar-zadeh, K. 2008, A Polyaniline/WO_3 Nanofiber Composite-based ZnO/64◦ YX $LiNbO_3$; SAW Hydrogen Gas Sensor; Synthetic Metals, Vol.158, pp. 29-32.

[53] Arsata, R., Yu, X.F., Li, Y.X., Wlodarski, W., and Kalantar-zadeh, K.2009, Hydrogen Gas Sensor based on Highly Ordered Polyaniline Nanofibers, Sensors and Actuators B, Vol. 137, pp.529-532.

[54] Atashbara, M.Z., Sadek, A.Z., Wlodarski, W., Sriram, S., Bhaskaran, M., Cheng, C.J., Kaner, R.B., and Kalantar-zadeh, K. 2009, Layered SAW Gas Sensor based on CSA Synthesized Polyaniline Nanofiber on AlN on 64◦ YX $LiNbO_3$ for H_2 Sensing, Sensors and Actuators B, Vol. 138, pp. 85-89.

[55] Srivastavaa, S., Sharmaa, S.S., Agrawal, S., Kumar, S., Singh, M., and Vijay, Y.K. 2010, Study of Chemiresistor type CNT Doped Polyaniline Gas Sensor, Synthetic Metals Vol. 160, pp. 529-534.

[56] Srivastava, S., Sharma, S.S., Kumar, S., Agrawal, S., Singh, M., and Vijay, Y.K. 2009, Characterization of Gas Sensing Behavior of Multi-Walled Carbon Nanotube Polyaniline Composite Films, International Journal of Hydrogen Energy, Vol. 34, pp. 8444- 8450.

[57] Srinivasan, S.S., Ratnadurai, R., Niemann, M.U., Phani, A.R., Goswami, D.Y., and Stefanakos, E.K. 2010, Reversible Hydrogen Storage in Electrospun Polyaniline Fibers, International Journal of Hydrogen Energy, Vol. 35, pp. 225-230.

[58] Yang, L.-Y., and Liaua, W.-B. 2010, Environmental Responses of Polyaniline Inverse Opals: Application to Gas Sensing; Synthetic Metals, Vol. 160, pp. 609-614.

[59] Sadek, A. Z., Trinchi, A., Wlodarski, W., Kalantar-zadeh, K., Galatsis, K., Baker, C. and Kaner, R.B. 2005, A Room Temperature Polyaniline Nanofiber Hydrogen Gas Sensor, in SENSORS 2005: Proceedings of the 2005 IEEE Sensors conference, IEEE, Piscataway, N.J., pp. 207-210..

[60] Yadav, J.B., Jadhav, S.V., Puri, R.K., and Puri, V. 2008, Properties of Vacuum Evaporated Vapour Chopped Polyaniline Thin Film: Effect of Synthesis Method, Journal of Physics Conference Series, Vol. 114, pp. 012037-xxx.

[61] Mylvaganam, K., and Zhang, L.C. 2007, Fabrication and Application of Polymer Composites Comprising Carbon Nanotubes, Recent Patents Nanotechnol. Vol. 1, pp. 59-65.

[62] Bai, H., and Shi, G. 2007, Gas Sensors Based on Conducting Polymers, Sensors, Vol. 7,pp. 267-307.

[63] Genies, E.M., Boyle, A., Lapkowski, M., and Tsintavis, C.1990, Polyaniline: A Historical Survey, Synthetic Metals, Vol. 36, pp. 139-182.

[64] Negi, Y.S., and Adhyapak, P.V., 2002, Development in Polyaniline Conducting Polymers, Journal of Macromolecular Science-part-C polymer Review, Vol. 42, pp. 35-53.

[65] Conn, C., Sestak, S., Baker, A.T., and Unsworth, J.1999, A Polyaniline-Based Selective Hydrogen Sensor, An International Journal devoted to Electronanalysis, Sensors, Bioelectronic device. 1999, Vol. 10, pp. 1137-1141.

[66] Sadek, A.Z., Trinchi, A., Wlodarski, W., Kalantar-zadeh, K., and Galatsis, K. 2006, A Room Temperature Polyaniline Nanofiber Hydrogen Gas Sensor, IEEE Xplore, Print ISBN:0-7803-9056-3, DOI: 10.1109/ICSENS.2005.1597672.

[67] Sadek, A.Z. Wlodarski, W., Kalantar-Zadeh, K., Baker, C., and Kaner, R.B. Doped and Dedoped Polyaniline Nanofiber Based Conductometric Hydrogen Gas Sensors, Sensors and Actuators A: Physical, Vol. 139, pp. 53-57.

[68] Laith Al-Mashat, Koo Shin, Kourosh Kalantar-zadeh, Johan D. Plessis, Seung H. Han, Robert W. Kojima, Richard B. Kaner, Dan Li, Xinglong Gou, Samuel J. Ippolito, Wojtek Wlodarski, 2010, Graphene/Polyaniline Nanocomposite for Hydrogen Sensing, J. Phys. Chem. C Vol. 114, pp. 16168-16173.

[69] Arsat, R., Yu, X.F., Li, Y.X., Wlodarski, W., and Kalantar-Zadeh, K. 2009, Hydrogen Gas Sensor Based on Highly Ordered Polyaniline Nanofibers, Sensors and Actuators B: Chemical Vol. 137, pp. 529-532.

[70] Sandaruwan, C., Herath, H.M.P.C.K., Karunarathne, T.S.E.F., Ratnayake, S.P., Amaratunga, G.A.J., and Dissanayake, D.P. 2018, Polyaniline/Palladium Nanohybrids for Moisture and Hydrogen Detection, Chemistry Central Journal, Vol. 93, pp. 1742-xxx.